Deep Sea Research in press 6 March, 1996

Appendix 6

# Calcification Rates in the Equatorial Pacific along 140°W

William M. Balch
Bigelow Laboratory for Ocean Sciences
P.O. Box 475
McKown Point
W. Boothbay Harbor, ME 04575

Katherine Kilpatrick
Division of Meteorology and Physical Oceanography
Rosenstiel School for Marine and Atmospheric Sciences
University of Miami
4600 Rickenbacker Causeway
Miami, FL 33149-1098

Running Head: Calcification in the Equatorial Pacific

Abstract

The calcite standing stock, calcification rate, concentrations of detached coccoliths and plated coccolithophore cells were determined in the equatorial Pacific along 140°W, between 12°N and 12°S latitude, during August and September 1992. Continuous surface optical and fluorescence measurements also were taken along this transect. Integrated calcification ranged between 3 and 12% of the total carbon fixed into particulate matter. Calcification exceeded 50% of the total fixed carbon (per unit volume) at specific depths from the northern-most oligotrophic stations. A pronounced subsurface peak in suspended calcite was noted near the equator. Calcification was considerably more patchy than photosynthesis. Normalizing the calcification rates to the surface area of calcite-producing species provided an estimate of the extracellular calcite flux rates. These results showed that the populations from the equator to 3°N at 60m depth, and near the surface from the equator to 9°S were the most active calcite producers. Underway estimates of light scattering showed the importance of upwelling for bringing cold, clear, relatively particle-free water to the surface, followed by growth and calcite production as the water warmed. When temperatures reached their upper range ( about 28.8°C), light scattering decreased again, presumably as growth slowed and particles sank. Integrated calcification estimates averaged over the equatorial region were compared to sediment trap data; the results suggest significant disappearance of calcite particles in the top 1000m, above the lysocline. One hypothesis to explain this is that dissolution occurred in microzones where decomposition of reduced organic matter lowered the pH sufficiently to dissolve calcite.

Introduction

Calcification in open ocean systems is poorly understood from ecological and biogeographical perspectives. Most calcification studies have been performed on calcifying macroalgae and corals due to their easy access from shore (e.g. Wefer, 1980; Kawaguti and Sakumoto, 1948). Studies of foraminiferal calcification, an important source of calcite for some course-grained sediments, are more difficult due to problems in laboratory culturing, lack of knowledge about life cycles, as well as finding sufficient material at sea (Be et al., 1977; ter Kuille and Erez, 1987 ). Coccolithophore calcification, a major source of calcite sediments in the world ocean (Milliman, 1993), has been well studied in the laboratory (e.g. Paasche, 1963) but direct, field estimates of calcification are few.

It has long been recognized that coccoliths contribute a major portion of the calcite content of pelagic sediments (Lohmann, 1908; Bramlette, 1958) and the distribution of many coccolithophores in surface waters matches their sediment distribution (McIntyre and

Be, 1967) except when preservation is poor. Atlantic waters are characterized by low dissolved $CO_2$, a deep calcium compensation depth (CCD) and good calcium carbonate preservation. However, the Indian and Pacific deep waters are generally characterized by relatively high dissolved $CO_2$ concentrations, high alkalinities, a shallow CCD, and low $CaCO_3$ preservation (Berger, 1971). In regions of high carbonate supply, the CCD can be depressed (the equatorial Pacific is such an example). Arrhenius (1952) first described significant variability in the calcite content of sediments, either due to changes in productivity or changes in dissolution (see also Cwienk and Leinen, 1985 and Samthein et al., 1988 for discussion of burial of biogenic phases). Broecker and Peng (1982) globally set the ratio of deposited calcite to surface-produced calcite as about 1:7, although this value will vary regionally as a function of the lysocline depth relative to the bottom depth. It is generally thought that calcite represents a progressively larger fraction of the total carbon flux as particles sink into deep water (see figure 1 from Westbroek, 1993).

Broecker and Peng (1982) estimate that, on a global basis, 1 mole of calcium carbonate is formed for about every 4.5 moles of organic carbon (i.e. 18% C is as calcium carbonate). In practice, any carbon fixed into calcium carbonate during bottle incubations is usually dissolved by acid fuming during analysis (Parsons et al., 1984); thus, information about this large carbon fraction is not included in production estimates. Moreover, little is known about coccolithophore patchiness scales in the horizontal and vertical dimensions. While large-scale variability (biogeography) is of more applicability to interpreting the sedimentary record, smaller scales of variability are important for understanding the physiological ecology of coccolithophores. Taxonomic studies have revealed vertical scales of variability in coccolithophore standing stock with resolution of about 20m (e.g. Okada and Honjo, 1973; Okada and McIntyre, 1977; Reid, 1980) . Few data are available concerning horizontal variability of coccolithophores in surface waters, at scales smaller than 100 km. Basin scale variability can be inferred from sedimentary distributions in the Atlantic (MacIntyre and Be, 1967) and the same probably applies to other ocean basins. Based on cell counts, Okada and Honjo (1973) showed in the Pacific Basin that coccolithophore biomass is highest at high latitudes, decreasing in temperate and subtropical regions, and then increasing again in the equatorial zone. Mesoscale blooms of coccolithophores also have been observed from space, allowing estimates of their scales of variability with resolution down to length scales of kilometers (Holligan et al., 1983; Balch et al., 1991; Aiken and Bellan, 1990; Holligan et al., 1993; Brown and Yoder, 1994a&b). Note, these bloom studies provided mostly information about the concentration of suspended coccoliths of *E. huxleyi*, not its biomass. This is because calcite coccoliths are highly visible from space due to their unique light scattering properties. Rates of

production of these suspended calcite particles also are not well understood in nature (but see examples in Balch et al., 1992 and Fernandez et al., 1993).

Geological studies of the equatorial Pacific have shown it to be a region of significant calcite sedimentation (Van Andel, 1975). Calcite represents >50% of the sediments by weight west along the equator to 158°W, with a zonal distribution from about 7°N to more than 15°S. The region of >70% calcite sediments is more restricted longitudinally, extending from 125°W to 157°W, then diminishing eastward along the East Pacific Rise. The latitudinal extent of the >70% calcite sediments is greatest at 135°W to 140°W (5°N to 15°S). Clearly, in the Equatorial Pacific, the majority of the sinking flux of biogenic carbon is being buried as calcium carbonate, not organic carbon (Van Andel, 1975).

*Geochemical estimates of calcification*

Most of the open ocean estimates of calcification in surface waters are indirect estimates by geochemists. They are based on measurements of inorganic carbon and nitrate over vertical length scales of hundreds of meters, and time scales of months (e.g. Broecker and Peng, 1982). Such data, combined with estimates of upwelling velocities allow estimation of the rates of photosynthesis and calcification. Alkalinity represents the extra positive charge that is balanced with $HCO_3^-$ and $CO_3^=$ to achieve electrical neutrality. The production of organic matter in photosynthesis is associated with a *decrease* in total carbon dioxide ($\Sigma CO_2$), and an *increase* in alkalinity (due to the uptake of $NO_3^-$ ). Calcification on the other hand, *reduces* the $\Sigma CO_2$, and removal of $Ca^{++}$ also removes 2 equivalents of positive charge. The net result is that during calcification, the decrease in alkalinity is twice the decrease in $\Sigma CO_2$. This appears in the equation for calculating calcification (Broecker and Peng, 1982):

$$\Delta C_{CaCO3} = (\Delta Alk + \Delta NO_3)/2 \qquad (1)$$

where $\Delta C_{CaCO3}$ represents the change in calcite carbon from the deeper water to the euphotic zone ($\mu mol\ kg^{-1}$), $\Delta Alk$ ($mEq\ kg^{-1}$) represents the vertical decrease in alkalinity from the deep water to the euphotic zone and $\Delta NO_3$ ($mM\ kg^{-1}$) represents the vertical decrease in nitrate from the deep water to the shallow water. This is to be contrasted with the geochemical production of organic carbon which is calculated using equation 2:

$$\Delta C_{org} = \Delta\Sigma CO_2 - \Delta C_{CaCO3} \qquad (2)$$

where $\Delta C_{org}$ represents the production of organic matter in surface waters, and $\Delta\Sigma CO_2$ represents the decrease in total inorganic carbon going from deeper water to shallow water as primary production occurs. Note that primary production and calcification have opposing effects on the dissolved inorganic carbon supply; photosynthesis consumes $CO_2$, calcification consumes two bicarbonate molecules, and produces one molecule of calcium carbonate and one molecule of $CO_2$.

As an example of calcification rates predicted by the above equation 1, we have applied the GEOSECS data from station 334 in the Equatorial Pacific (0° 3'N x 124° 34'W; 27 May 1974). An upwelling rate of about 1 m $d^{-1}$ has been reported in this region but it is confined to the top Ekman layer (about 50-100m in this region) with significant deep meridional geostrophic flow from the north and south (Wyrtki, 1981). Therefore, we base euphotic estimates of calcification on geochemical changes in this vertical depth range. The value of $\Delta C_{CaCO3}$ at the equator, based on equation 1, is 17.08 μmol $l^{-1}$ after normalizing for salinity differences and correcting for density. Multiplying these values by the average regional upwelling velocity gives integral calcification values of 17.08 mmol C $m^{-2}$ $d^{-1}$ or 6.24 mol $m^{-2}$ $y^{-1}$. These data, applied to equations 1 and 2, predict that over 10% of the carbon fixed into particles in this highly productive region would be as calcium carbonate. There are no direct measurements of calcification to verify this, however.

Calcite production does not require nitrogen, hence, calcification technically should not be included in new production (sensu strictu Eppley and Peterson, 1979). Calcite does represent a large fraction of the export carbon, however. The new production "f" ratio (fraction of total production associated with nitrate uptake) from the tropical Pacific is about 0.14 (Pena et al., 1994) , which is about the same as estimates of carbon fixed into calcite in this specific region. The importance of the calcite production over new production becomes even more obvious, when one considers that most of the new production is never buried in sediments, but is remineralized enroute to the sea floor. If the global average primary production is between 20-30 gt carbon $y^{-1}$, and organic production is 4.5 times the calcite production (Broecker and Peng, 1982), then global calcite production will range from 4.4 to 6.7 gt carbon $y^{-1}$. This spans the global calcite production estimate of Milliman (1993; 5.2 gt carbon $y^{-1}$). In the Equatorial Pacific box described by Wyrtki (1981; 1.1 x $10^{13}$ $m^2$), the geochemical estimate of total calcification would be about 0.8 gt carbon $y^{-1}$, which represents 12-19% of global calcite production, and is of the same order of magnitude as new production in the equatorial Pacific (Chavez and Barber, 1987).

The rationale for this Equatorial Pacific study was based on the importance of sinking calcite to 1)export carbon fluxes, and 2) the total global calcification burial. Clearly, little is known about the factors that affect calcification by coccolithophores in

space and time. Better knowledge of the rate of crystalization of this mineral, coupled with mass balance, indirectly provides limits for the euphotic loss terms, sinking and dissolution. The following study represents the first direct measurements of surface calcification rates in the equatorial Pacific, a region where calcification is an important fraction of the flux of carbon from surface waters to deep sediments.

## Methods

### *Cruise Details*

All measurements were made during the 1992 Survey II cruise aboard the R/V Thompson (5 August-18 September, 1992) from Hawaii to Tahiti. Fifteen stations along 140° W were occupied, stopping at 12° N, 9° N, 7° N, 5° N, 3° N, 2° N, 1° N, 0° , 1° S, 2° S, 3° S, 5° S, 7° S, 9° S, 12° S. A description follows of the measurements made at each station (as vertical profiles). These measurements were also made on surface underway samples every 1-2 hours of the transit.

### *Calcification Measurements*

Water for vertical profiles was sampled using a trace-metal clean rosette, equipped with eight 30 liter GO-FLO sampling bottles. Samples for calcification were generally taken between midnight and 0300 local time to avoid light shock to the phytoplankton. Water from each depth was poured into two 250 ml polycarbonate bottles after 5 bottle rinses. Gloves were used during all sampling and handling. Calcification was measured using the technique of Paasche (1962, 1963). 40μCi of $^{14}C$ bicarbonate (radiochemical purity>99.9999% as determined in our laboratory) was added to each sample afterwhich the bottle was incubated in situ or in incubators on the ship's deck. Subsamples of 100μl were taken from two bottles of each series for total 14C counts, and mixed with 100μl of phenethyl amine, mixed, and 7ml Ecolume scintillation cocktail was added. For in situ incubations, two bottles were placed in each of eight nylon monofilament bags, attached to a floating spar buoy. They were incubated at 1, 12, 21, 34, 45, 60, 79, and 118m (approximately the 100, 50, 30, 14, 7, 3, 1, and 0.1% light depths) for 24 hours. Simulated in situ incubations were done in a series of Plexiglas tanks on the fantail of the ship with temperature matched to the in situ temperature within 1°C. The tanks had blue Plexiglas walls and tops to mimic the spectral quality of the water. Light quantity was controlled by neutral density screen bags around the bottles. After 24h, all samples were retrieved. Four 50 ml samples from each 250 ml bottle were filtered through 0.4 μm Nuclepore filters, rinsed 5 times with filtered sea water with low vacuum, then the filter tower was removed and the filter given a careful "rim rinse" to wash off any radiolabeled

bicarbonate activity, being careful that all the rim rinse was drawn through the filter. All filter manipulations were done using acid-cleaned/seawater-rinsed forceps to avoid contamination. For every four replicate filters, two were added directly to 7mL of Ecolume scintillation cocktail. The other two were placed in a desiccator containing 25ml of concentrated HCl for 4 minutes, then removed and placed in a scintillation vial with 7 ml of scintillation cocktail. Previous studies have shown that this fuming process was sufficient to remove any calcite on the filter (Balch et al., 1992). Radioactivity was measured using the external channels ratio method. All samples were counted for 5 minutes. The equations of Parsons et al. (1984) were used to calculate the uptake rate of carbon into organic matter/calcite, isotope discrimination was assumed to be 5%.

*Suspended Calcite Analyses*

Suspended calcite was measured on pre-combusted GFF filters using the technique described by Holligan et al (1993). One liter samples were filtered through pre-combusted Whatman GFF 25mm filters, the filters were rinsed several washes with filtered seawater. Then one rinse of 20mM borate buffer, pH 8.0 to remove any calcium ions in sea water before freezing the filters at -20$^{o}$C. Samples were extracted by adding ml -50% trace-metal clean hydrochloric acid to tubes containing the filters. They were incubated overnight at 40 $^{\circ}$ C in a water bath. 8 ml of 1% lanthanum chloride was added to each tube, followed by centrifugation to remove any filter fragments. The supernatant was then injected into a Perkin Elmer model 2380 flame photometric atomic absorption spectrometer, measuring absorption at 422.7 nm with a 10 cm flame. Calibration curves were prepared using commercial calcium standard from Fisher Scientific. Blank filters were prepared towards the end of the cruise by mounting identical pre-combusted filters in the filter tower apparatus, applying vacuum, and adding GFF-filtered seawater to wet the filter, and identical rinsing and preparation techniques as described above.

*Chlorophyll*

Chlorophyll concentration was measured as described by Yentsch and Menzel (1963) subsequently modified by Holm-Hansen (1965). For all samples, 250 ml was filtered through GFF filters, the filters were extracted in 90% acetone in scintillation vials overnight at 4$^{o}$C, the acetone was decanted into a cuvette and chlorophyll fluorescence measured with a Turner Designs fluorometer.

*Continuous along-track measurements*

A flow-through system was attached to the ship's clean stainless steel seawater supply. The underway system consisted of a Turner 111 fluorometer with flow-through door, an Interoceans model 541 temperature/conductivity probe. Water passed through a continuous 90° light scattering detector described elsewhere by Kilpatrick et al (1994). Basically, 90° light scattering was monitored over 3 minute cycles as a peristaltic pump moved water through a flow-through cuvette at a rate of 11 ml $min^{-1}$. During half the cycle, a second pump injected 1% glacial acetic acid to lower the pH to 5 and dissolve any suspended calcium carbonate. When the signal stabilized, the acidified reading was subtracted from the unacidified, raw reading. The difference in readings represented acid-labile scatter which was calibrated to suspended calcite in the laboratory. At a steaming speed of 11 knots (required for other towed instruments) , the underway system sampled about once every kilometer.

*Cell Counts*

Samples for cell counts were taken at every station and preserved with 3 ml buffered Lugols solution in 60ml brown glass bottles. Samples were stored up to 1.5 years before enumeration; bottles were taken at random for counting and the bottle identification numbers were not known to the microscopist until after the count. Ten ml of each sample was poured into a settling cylinder which rested over a Palmer Maloney counting chamber (the cylinder was lightly greased with silicon grease to seal it to the counting slide. Particles were allowed to settle onto the counting slide for 24 hours. Then the upper cylinder was removed by slowly sliding if across the Palmer Maloney slide and draining it into an underlying beaker. The settled sample was examined with an Olympus BH2 microscope equipped with polarization optics which allowed the enumeration of calcite birefringence. Detached coccoliths and 3 sizes of plated coccolithophores were counted (<10um, 10-20um, 20-30um diameter). The total numbers of coccoliths $ml^{-1}$ were calculated based on the counts of single, detached coccoliths as well as estimates of coccoliths on cells and in aggregates. Cells and aggregates were binned according to the size categories given above for cells. Approximate numbers of coccoliths were estimated for cells or aggregates based on microscopic examination: <10μm =16 coccoliths, 10-20μm = 100 coccoliths, and 20-30μm =200 coccoliths. Each particle type was enumerated in the chamber up to a maximum count of 200 particles, otherwise the entire chamber was counted. Naked coccolithophores were difficult to identify using this technique, and were not included in the counts. In order to relate the physiological measurements to the microscopic counts, an extracellular calcite flux was calculated by dividing the calcification

rate by the plated coccolithophore cell surface area assuming spheres of the diameter given above (units of $m^2$ cell surface area ($m^3$ seawater)$^{-1}$).

Results

Distributions of detached coccoliths and plated coccolithophores covaried with highest concentrations observed between the equator and 3°S (highest at 1°S) and at 7°N and 7°S (Fig. 1). In general, highest concentrations within the euphotic zone were shallower than 50m. The concentration of both coccoliths and cells varied over 3 orders of magnitude in the study area ; the least squares relationship between detached coccoliths and plated cells was: Log coccoliths = 0.93 * Log Plated Coccolithophores + 0.95 ($r^2$=0.61; Fig. 2). Based on this relationship, the ratio of detached coccoliths to plated coccolithophores varied between 5 and 8. This did not include clumps of detached coccoliths which sometimes were abundant, but impossible to count accurately. Unidentified 0.5um birefringent particles were extremely abundant (up to 75,000$mL^{-1}$) at about 40-50 meters between 5°S and 4°N as well as some deeper at 100m from 10°S to 4°N (Fig. 3). Attempts to examine them using scanning electron microscopy were fruitless as they proved to be extremely fragile.

Photosynthesis rates showed a broad, asymmetrical maximum centered at 2°N. Meridional gradients in primary production were considerably stronger north of the equator, with the steepest gradient observed between 2°N and 3°N, at the "Great Front" (Fig. 4a). This was an open-ocean front, associated with the convergence between the westward-flowing south equatorial current, and the eastward-flowing north equatorial counter current (Yoder et al., 1994). Calcification did not show the same pattern as primary productivity, and was considerably more patchy. Highest values were seen at the equator. The lowest calcification rates were observed north of about 7°N (Fig. 4b). Suspended calcite was highest near the equator, just below the depth of peak calcification (Fig. 4c). Calcite data from 7°-12°N were lost.

It should be noted that the estimates of suspended calcite concentrations using water from Niskin bottles tended to be higher than water sampled from in situ pumps. Suspended calcite concentrations measured by large-volume pumps were about a factor of 2-5 times less than values from discrete bottles (J. Bishop, personal communication). This was also true of the particulate organic carbon samples (Ducklow, personal communication). We cross-checked the precision of our atomic absorption technique by running sub-samples from the large volume filtration system of J. Bishop, and our results were within 10%. Thus, the discrepancy between large-volume samplers and Niskin bottles rests in how the samples were taken, rinsed or stored. Given that the absolute

accuracy of either method is poorly defined, it is impossible to resolve this difference and we report our results from the Niskin bottles.

A plot of calcification versus photosynthesis for in situ and simulated in situ incubations showed that calcification rates were equal or greater than photosynthesis rates in the most oligotrophic water. In higher productivity water, calcification was generally about 10% of photosynthesis, with maximum calcification rates of about 0.25 μmol C $m^{-3}$ $d^{-1}$ (Fig. 5).

Calcification, photosynthesis, and suspended calcite concentrations were integrated to the 0.1% light depth using trapezoidal integration. General patterns of integrated calcification and photosynthesis showed that calcification was usually about 5-10% of total carbon production, which was highly latitudinally dependent. Integrated calcification and photosynthesis were highest at 2°N (Fig. 6a) with a gradual decrease south of the equator, and steeper decline north of the equator. Integrated calcite standing stocks were greatest at 1°S (Fig. 6b). Turnover, estimated by dividing the calcite standing stock by its rate of production, was almost always less than about 10d except for the data calculated from the in situ incubations at 1°S (Fig. 6c). Integrated calcification was between 3% and 12% of the integrated photosynthesis (Fig. 7).

The abundance of detached coccoliths was compared with the surface area of the plated coccolithophore cells that presumably generated them (Fig. 8). The expected relationship for coccoliths of different radius was generated assuming that all detached coccoliths originated from the plated coccolithophores, and that those coccoliths originally completely covered the cells in a single layer. Calcification rates were also normalized to the surface area of plated cells (calculated from the cell counts). The results showed that the greatest rates (> 2 mol C $m^{-2}$ cell surface area $d^{-1}$ ) were found between the equator and 3°N at about 60m, and also at 9°S at the surface (Fig. 9). Most of the study region had rates <0.25mol C $m^{-2}$ cell surface area $d^{-1}$. Calcification rates normalized to the numbers of plated cells showed no trends, probably due to the large range of cell sizes seen in the samples.

*Underway transect results*

The underway data (figure 10) showed that salinities increased along the transect from 12°N to 12°S, with a pronounced low of 34.75 associated with the "great front" and a broad region of 35.25-35.5 salinity from the equator to 5°S associated with the south equatorial current. Lowest salinities of about 34.25 were seen from 9-12°N. Underway temperature values were highest at 7-9°N, and coolest south of the convergence front at 2°N (lowest temperature of the transect was ~24.5°C) . A temperature drop of about 1°C

was observed at 9°N. Surface temperatures warmed from 2°N to 8-9°S, then cooled about one degree at 12°S. Chlorophyll fluorescence a) increased from 6°N to 5°N, b) had a sharp maximum just north of the 2°N convergence front, and c) had lesser peaks at 1.5°N and the equator. From the equator to 6°S, chlorophyll values ranged from 0.1-0.2 mg $m^{-3}$ and the beginning chlorophyll value from one transect rarely matched that from the end of the previous transect; this indicated that conditions were changing while the ship was on station for 2-3d. Small, well-defined chlorophyll peaks of 0.15 mg/$m^3$ were observed at 6°S and 9°S. Trends in total 90° volume scattering generally covaried with temperature, with the exception of two regions at 2°N and 8°N. For interpretation of the total 90° scattering signal, it is important to caution that an impeller pump supplied the water to the flow-through system and extremely large cells such as the diatom, *Rhizosolenia castracanei,* from the "great front" (Yoder et al., 1994) may have not survived intact. The difference between total and acidified 90° volume scattering (calcite-dependent scattering) was highly variable from 12°N to 5°N. At 2°N and 2°S, large peaks of acid-labile light scatter were observed. In the southern part of the transect (6°S-12°S), the acid-labile scatter values were slightly negative (~-0.01V).

The same underway data were plotted on temperature/salinity coordinates in figure 11 to relate the observations to specific water masses. The surface waters between 12°N and 12°S had sigma-T values ranging from 21.5 to 23.5 respectively (Fig. 11a). The same data, with isopleths of latitude showed the low density water in the north part of the transect, and coldest water observed just north of the equator (~1°N; Fig. 11b). The chlorophyll data, superimposed on the temperature/salinity space showed the presence of the intense *Rhizosolenia castrecanii* bloom at 2°N (Yoder et al., 1994) as well as a minor peak in the cool, $\sigma_{t23.5}$ water upwelled at the equator. Acid labile 90° volume scattering data, plotted in temperature/salinity space again were extremely patchy, but several peaks were observed well within the upwelled equatorial water at 1°N, and some patches at about 12°S (Fig. 11d). Total 90° volume scattering showed an unexpected pattern, almost inverse to the chlorophyll pattern, with values lowest at the great front and equator, and higher in more oligotrophic parts of the transect (Fig. 11e).

A different way to examine the total 90° light scattering was to plot it against temperature (Fig. 12). The results showed lowest 90° scattering in the cold upwelled water, reaching a maximum at about 28.8°C, then abruptly declining up to 29°C. A line, drawn by eye, illustrates this trend.

The above results have been submitted to the U.S.-JGOFS data system.

## Discussion

*Horizontal and Vertical Distribution of Coccoliths and Coccolithophores*

Two aspects of the spatial distribution of coccoliths are worthy of note. The absolute abundance of detached coccoliths (plus plated coccolithophores) peaked in the waters south of the equator, which was recently upwelled and of moderately low chlorophyll (Fig. 11). This was in agreement with the observations of Okada and Honjo (1973). Furthermore, the locations of the highest coccolith abundance and calcite concentration generally, but not always, corresponded to the locations of peak calcification (compare Figs. 1a, 1b, 4b and 4c). Patches of water with high calcite-dependent, 90° volume scattering were observed in regions of moderate chlorophyll between 1°N and 2°N, south of the "great front" (Fig. 10). While coccolithophores are usually thought to tolerate low nutrient, low iron water (Kramer and Ryther ,1960), our data showed patches clearly associated with recently upwelled water (Fig. 11d). This might be explained using the mandala derived by Margalef (1978) in which he placed coccolithophorids between the dinoflagellates (selected for low turbulence, low nutrient environments) and the diatoms (selected for high turbulence, high nutrient environments). The flagellated life stage of coccolithophores appears to be a relatively minor part of its overall life cycle, and most of the time, cells are covered by calcite plates giving them high sinking rates. Thus, Margalef rationalized that coccolithophores require moderate turbulence to remain aloft in the water column. Recently upwelled water, in the process of stratifying, might provide just such conditions.

The optical data indicated fairly uniform but low concentrations of coccoliths in the north end of the transect and extremely low values in the southern surface waters. Slightly negative volume scattering in the south end of the transect, suggested that there may have been some fragmentation of fragile cells during the pH shift, such that the acidified volume scattering values were slightly greater than those from raw seawater. These same trends were also observed in the cell and coccolith count data (Fig. 1), albeit with considerably lower horizontal resolution (one vertical profile every 300km).

The unidentified birefringent particles (Fig. 3) may have been holococcoliths, rhombohedral crystals produced by some Prymnesiophytes. This remains unconfirmed due to lack of scanning electron micrographs, however. Most striking was the coherence in the pattern given that samples were randomly counted (and sample identities were unknown to the microscopist until after the counts). It should be noted that these particles corresponded to patches of high suspended calcite concentration (Fig. 4c), 30-50m above the core of the equatorial undercurrent.

*Calcification and Photosynthesis*

One of the most striking results of the calcification measurements was that there were several areas, such as at 12°N, at 20m depth, where calcification and photosynthesis were equal (Fig. 5) . This was even more striking when one considers that calcification was performed by only a few species, while photosynthesis was performed by all phytoplankton. Another interesting result concerned the short turnover times of calcite in the euphotic zone (3-10d), unexpected for a non-nutritious particle (Fig. 6c). Only at 1S, was the turnover time 50d due to the very high standing stock of calcite. These data, combined with the cell counts (Fig. 1) suggest that grazing was partially responsible for the rapid calcite disappearance. We have previously observed similar rapid turnover in the central north Atlantic and Gulf of Maine (unpublished data). This interpretation was consistent with the model of Honjo (1976) which listed zooplankton fecal pellets as the major vehicle for carrying micron-sized sinking calcite particles to depth.

Calcification normalized to the area of plated coccolithophore cells provided insight into where extracellular calcite fluxes were most rapid. The scale of these measurements ranged over two orders of magnitude. Admittedly, this analysis was taxonomic in only the broadest sense, since we only enumerated the numbers and sizes of plated coccolithophores, not their species identification. Even if we had identified cells to the species level, it would have been impossible to unequivocally determine which ones were responsible for the highest flux rates because coccolithophore populations were rarely monospecific. Another limitation of this analysis was that it assumed that only calcifying cells had visible calcite birefringence. Nevertheless, there was the possibility that certain calcifying cells had not yet accreted sufficient coccoliths to make their birefringence clearly visible in the microscope, or they simply had detached all of their coccoliths. Our analysis assumed that such cells represented a small fraction of the total coccolithophore biomass.

The mean extracellular calcification flux rate at all stations was 0.24 mol C ($m^2$ cell membrane)$^{-1}$ $d^{-1}$ (standard deviation= 0.44 mol C ($m^2$ cell membrane)$^{-1}$ $d^{-1}$). This average was somewhat biased by samples from a few select depths, with rates 10X higher than the average (e.g. 60m depth and 1°N). In fact, most of the study area had flux rates < 0.1mol C ($m^2$ cell membrane)$^{-1}$ $d^{-1}$. It is useful to compare these rates to data from *Emiliania huxleyi*. Our previous laboratory results showed that clone 88E of this species had an average diameter of 4.75μm (average cell surface area without coccoliths= 70.9$\mu m^2$; See table 2 from Balch et al., 1993) and calcification rates of 10-60 fmol cell$^{-1}$ $h^{-1}$ (Balch et al., 1992). Therefore, the range of extracellular calcification flux rates was 3.39 x $10^{-3}$ to 2.00 x $10^{-2}$ mol C ($m^2$ cell membrane)$^{-1}$ $d^{-1}$, over 10X lower than what we observed in the equatorial Pacific . As a cross check, the same analysis was done for a

coccolithophore bloom in the Gulf of Maine in 1989, at station 4, 5m (see Balch et al., 1992). The coccolithophore concentration at this station was 1550 cells $ml^{-1}$ and the calcification rate was 1mmol $m^{-3}$ $d^{-1}$. Using the same diameter for *E. huxleyi* given above, the extracellular calcite flux rate was 9.1 x$10^{-3}$ mol C ($m^2$ cell membrane)$^{-1}$ $d^{-1}$, again much lower than the Equatorial Pacific data, yet quite similar to the data from our laboratory experiments. Our conclusion from these comparisons was that *E. huxleyi*, in laboratory cultures or monospecific blooms, can be characterized by a moderately low extracellular calcification flux rate, and probably another coccolithophore species was responsible for the higher extracellular calcite flux rates in the equatorial upwelling region. Typical coccolithophore species in this region are *E. huxleyi, Cyclococcolithina fragilis, Cyclococcolithina leptoporus, Gephyrocapsa oceanica, Umbellosphaera hulburtiana, Umbellosphaera irregularis*, and *Discosphaera tubifera* (see Okada and Honjo, 1973).

The estimated area of plated coccolithophore cells plotted against the number of detached coccoliths had a slope equal to the effective area per coccolith. If one assumes that the coccoliths were shaped like flattened discs, then the lower limit of the data distribution (Fig. 8) represented coccoliths of about 1μm radius, the size of the smallest coccoliths of *Emiliania huxleyi* and *Gephyrocapsa oceanica*. The high end of the distribution implied coccoliths having 8μm radii. The least-squares-fit slope to these data (Log plated cell area m-3 = (0.50 (log (detached coccolith concentration))) - 4.0) was about half of the slope of the isopleths shown in Fig. 8; while this could have been fortuitous, it could have been due to coccolith size changing as a function of coccolith concentration. That is, when the concentration of detached coccoliths was low, the mean coccolith radius was about 4μm and when the concentration was high, the mean radius was about 1μm. As stated before, such an interpretation does not take into consideration that coccoliths may have been layered on cells (Balch et al., 1993). Since the lower limit of these data closely matched the minimum size of heterococcoliths of the smallest species (see Reid (1980) or Okada and Honjo (1973) for examples of Pacific Ocean coccolithophore species) then the idea that cells were covered by one layer of coccoliths seems reasonable.

*Light scattering by particles and upwelling*

The results of the underway measurements showed that in the *Rhizosolenia* bloom at the "great front", the total volume scattering at 90° was unexpectedly less than in adjoining waters. To the contrary, just north of the equator, in the core of the upwelled water, a small peak in chlorophyll was associated with increased 90° volume scattering. While the large Rhizosolenia may have not survived the impeller pump, it is more likely that the 90° volume scattering was contributed mostly by very small particles, not the 400-

500μm length *Rhizosolenia* cells, and these small scattering particles were at minimal concentration at the front whereas they were more abundant in the upwelling waters. Morel and Ahn (1991) have previously shown that heterotrophic bacteria and other sub-micron particles are extremely efficient backscatterers of light, more than larger algae. Thus, 90° volume scattering could have been dominated by small particles instead of large diatoms. This interpretation was also buttressed by the fact that similar patterns were observed in the underway beam attenuation and fluorescence measurements made with the Undulating Optical Recorder (UOR; Trees and Aiken, personal communication). Their data showed the presence of the same chlorophyll features that are shown in figure 11 as well as similar behavior of beam attenuation; it *decreased* in the *Rhizosolenia* feature and increased in the non-*Rhizosolenia* feature. It is important to caution that beam attenuation is more a function of total scattering than backscattering, and Morel and Ahn (1991) have shown that algal cells influence the total scattering coefficient more than backscattering coefficient.

A plot of total 90° volume scattering versus temperature indicated an asymmetrical curve reminiscent of temperature tolerance experiments done by others (Eppley, 1972). In such experiments, populations grew increasingly fast as temperature was raised, but above a threshold temperature, growth rates declined precipitously. In our data, the coldest upwelled water was associated with water having the lowest 90° volume scattering. The only exception was a small patch of water at 8.5°N that also had low scattering and a temperature of 27.5°C; this patch may have still represented water upwelled from a shallower depth, however (Fig. 10). The surface temperature where volume scattering decreased sharply was about 28.5°C and by 29°C, the total 90° volume scattering was the same as in the newly upwelled equatorial water. Our cell counts certainly showed that the species of phytoplankton varied over the transect, thus it was not possible to attribute this behavior to any one species undergoing thermal stress. Nevertheless, from a bio-optical perspective, the evidence suggested that the upwelled water surfaced relatively free of particles, particle formation occurred in the mid-temperature ranges and stopped above 28.5°C. Subsequent sinking of remaining particles caused the 29°C surface water to reach the clarity of the upwelled water.

*Synthesis: Sources and Fates of Calcite Production in the Equatorial Pacific*

These results provide insight into the biogeochemistry of calcium carbonate in the equatorial Pacific. Broecker and Peng (1982) showed with GEOSECS data that in the Pacific, the average ratio of biologically produced organic matter to biogenically produced calcite was 4.4 (not much different from their global ratio of ~4.5). Integral chlorophyll values from survey cruise II (JGOFS core data of B. Bidigare and J. Newton) were used

to calculate integral phytoplankton carbon, assuming a typical carbon:chlorophyll ratio of 75. Dividing these values by our observed integral calcite standing stocks gave ratios of organic to inorganic standing stocks with a large range, between 4 and 12 (with the exception of 1°S which had an anonymously low value of 1.5).

The conceptual model of Westbroek et al. (1993) predicted that the global ratio of photosynthesis to calcification is 20-30 and they showed how organic matter is gradually remineralized enroute to the sea floor until calcite far outweighed organic carbon, and the ratio of burial rates of organic to inorganic carbon into the geological archive was about 0.18 (See also Fig. 4 from Milliman, 1993). Our data suggested that in the equatorial Pacific, surface calcite production played a more important role than suggested by Westbroek (1993). This is because the ratio of integral photosynthesis to calcification was about 7-9 in the oligotrophic regions and about 8-32 near the equator, not 20-30. The average ratio for the entire data set was about 11. Such values were similar to the ratios of the standing stocks of organic carbon to calcite carbon. The main way to incorporate increased calcification into models such as that of Westbroek et al. (1993), without changing burial fluxes, is to increase calcite dissolution, either at the bottom or enroute to the sea floor.

The cell count data demonstrated a general decrease in the concentration of calcite coccoliths and cells in equal proportion below 60m depth (with the exception of one sample at 80m at 5°N; Fig. 1). Since these particles were well above the lysocline and calcium compensation depth (Seibold and Berger, 1982), dissolution should have been minimal, but, for reasons to be discussed, this possibility still cannot be discounted.

Detached coccoliths settle at extremely slow rates of about 0.1 m $d^{-1}$ so that incorporation into fast-sinking fecal pellets is the most likely vertical transport mechanism (Honjo, 1976). Two potential causes for the loss of coccoliths and coccolithophores below 60m are: 1) incorporation into fast-sinking fecal pellets by grazers or 2) dissolution. If the sinking pellet hypothesis is true, then our data do not suggest much discrimination by grazers between coccolithophores and their coccoliths since the ratio of coccoliths to plated cells (about 10:1; Fig. 2) did not change with depth. Had the ratio increased with depth, then one could have hypothesized that the plated cells were preferentially grazed. Lack of a vertical change in this ratio could also be attributed to dissolution, which presumably is the same for coccoliths detached or attached to cells.

It is reasonable to assume that grazing was the process repackaging coccoliths and transporting them downwards in fecal pellets, given that the estimated turnover time of the calcite was several days. However, calcite in fecal pellets should have been caught in sediment traps. The sediment trap data of Newton (in preparation) and Honjo et al.

(submitted) showed that a large fraction of the calcite flux disappeared in the top 3000m of the water column, which can be attributed to dissolution or horizontal advection of calcite particles from the trap sites. For example, the sediment trap data that most corresponded to the period of survey cruise II are from 10 -27 September, 1992 (time periods 14 and 15; Table 3 of Honjo et al., submitted). Note, as suggested by these investigators, this time period allowed 17d for the particles to sink from the surface to the traps. Averaging the Honjo et al. (submitted) flux data for all traps between 2000m and 3800m, within 5°N and 5°S, gave calcite flux rates of 535μmol $m^{-2}$ $d^{-1}$ (s.e.=43.3, n=11). Our average integrated calcification rates within 5°N and 5°S were 2750μmol $m^{-2}$ $d^{-1}$ (s.e.=11.5; n=9). If our assumption was correct, that is, that the calcification we measured was caught in the traps between 10 and 27 September, then some 4/5 of the calcite disappeared above the CCD (4700-5000m; Van Andel, 1975). At the equatorial station reported by Honjo et al. (submitted) their shallowest trap was deployed at 800m. The flux of calcite into this trap was 332 μmol $m^{-2}$ $d^{-1}$, not significantly different from the trap at 2284m (490μmol $m^{-2}$ $d^{-1}$). This argues that any calcite loss was occurring in the top 1000m of the water column.

One obvious explanation for the above results was that there was a mis-match of time and space scales; that is, the calcite that was caught in the sediment traps was not the same that we measured in surface waters. Milliman (1993) discussed the potential problems when comparing fluxes and accumulation rates of sediment traps and sediment cores due to the different time scales involved; the same could apply to comparisons of surface incubations and sediment trap data. Obviously, given the potential problems with sediment trap efficiencies, such data should be interpreted carefully. Nevertheless, the data of Honjo et al.(submitted) convincingly showed minimal temporal offset (<17d) between the surface and deep sediment trap collection rates, suggesting rapid settling fluxes. If dissolution indeed were occurring above the CCD, then one explanation was that calcite dissolved in microzones, perhaps where decomposition of reduced organic matter lowered the pH sufficiently to dissolve calcite (analogous to Emerson and Bender's (1981) model of calcite dissolution at the sediment-water interface). Obviously, there are some historical data contrary to this hypothesis (e.g. Berger et al., 1982), but if the hypothesis is true, then the role of calcification in transferring bicarbonate to the deep sea (Westbroek et al., 1993) should be reevaluated in the equatorial Pacific since much of the carbonate never reaches the CCD.

The importance of dissolution in the benthos is also addressed by Berelson et al. (1990). They showed deep water calcium carbonate dissolution rates in the equatorial Pacific (135-140°W) of about 300-500 μmol $m^{-2}$ $d^{-1}$. Berelson's measurements from the EqPac cruises (Berelson et al., in press) ranged from 450-650 μmol $m^{-2}$ $d^{-1}$ with highest

rates at 2°N. Such rates essentially are identical to the rates of delivery calculated by Honjo et al. (submitted). Thus, while most dissolution happened in shallow waters through some unknown mechanism, deep sedimentation of calcite balanced benthic dissolution. This would imply that no net accumulation of calcium carbonate currently is occurring in this region.

A final aspect of carbonate cycling that has arisen during this analysis relates to the fraction of calcite production that sinks to the sea floor. As mentioned above, the overall average integral calcification between 5°N and 5°S over the 32 days that those samples were taken was about 2750 $\mu$mol $m^{-2}$ $d^{-1}$. The ratio of calcite production to sedimentation was ~5, smaller than the global ratio of 7 cited by Berger (1971) and Broecker and Peng (1982). Clearly, if calcite dissolution was occurring in the upper water column instead of the deep sea, and one part in five reached the sediments instead of one part in seven, then equatorial Pacific carbon flux models need to be adjusted accordingly. The ramifications of such a difference would mean that, assuming the same surface calcification rate, 1) most of the bicarbonate produced during calcite dissolution would remain in the top 1000m instead of the deep sea, and 2) the larger fraction of surface calcification reaching the benthos would help maintain the balance between calcite sedimentation and burial in this important part of the world ocean.

Acknowledgments- The captain and crew of the R/V Thomas Thompson provided expert ship handling and logistical support. James Murray and two anonymous reviewers provided comments on an earlier draft. Susan Kadar provided vital pre- and post-cruise logistical support. This is contribution number 220 of the U.S. JGOFS program and contribution number 96003 of the Bigelow Laboratory for Ocean Sciences. This work was generously supported by the National Science Foundation (OCE-9022227), the Office of Naval Research (N00014-91-J-1048) and NASA (NAGW-2426 and NAS5-31363).

References


Aiken, J. and I. Bellan (1990) Optical oceanography: An assessment of a towed method, In: *Light and Life in the Sea*, P. J. Herring, A. K. Campbell, M. Whitfield, and L. Maddock, editors. Cambridge University Press, New York, pp. 39-57.

Arrhenius, G.O. (1952) Sediment cores from the East Pacific. *Swedish Deep-Sea Expedition Reports, 1947-48.*, **5**, 189-201.

Balch, W.M., P.M. Holligan, S.G. Ackleson, and K.J. Voss (1991) Biological and optical properties of mesoscale coccolithophore blooms in the Gulf of Maine. *Limnology and Oceanography*, **36**, 629-643.

Balch, W. M., P. M. Holligan and K. A. Kilpatrick (1992) Calcification, photosynthesis and growth of the bloom-forming coccolithophore, *Emiliania huxleyi.*, Continental Shelf Research, **12**, 1353-1374.

Balch, W.M., K.A. Kilpatrick, and P.M. Holligan (1993) Coccolith formation and detachment by *Emiliania huxleyi* (Prymnesiophyceae), *Journal of Phycology*, **29**, 566-575.

Be, A. W. H., C. Hemleben, O. R. Anderson, M. Spindler, J. Hacunda, and S. Tuntivate-Choy (1977) Laboratory and field observations of living planktonic foraminifera, *Micropaleontology*, **23**, 155-179.

Berelson, W. M., D. E. Hammond, and G. A. Cutter (1990) In situ measurements of calcium carbonate dissolution rates in the deep-sea sediments, Geochimica et Cosmochimica Acta, **54**, 3013-3020.

Berger, W. (1971) Sedimentation of planktonic foraminifera, *Marine Geology*, **11**, 325-358.

Berger, W., M., -C. Bonneau, and F. L. Parker. (1982) Foraminifera on the deep-sea floor: Lysocline and dissolution rate. Oceanol. Acta, **5**, 249-258.

Bramlette, M.N. (1958) Significance of coccolithophorids in calcium carbonate deposition, *Bulletin of the Geological Society of America*, **69**, 121-126.

Broecker and Peng (1982) *Tracers in the sea.* Lamont-Doherty Geol. Obs., Columbia University , New York. 690 pp.

Brown, C. and J. Yoder (1994a) Distribution pattern of coccolithophorid blooms in the Western North Atlantic. Cont. Shelf Res., **14**, 175-198.

Brown, C. W. and J. A. Yoder (1994b) Coccolithophorid blooms in the global ocean. J. Geophys. Res. **99**, 7467-7482.

Chavez, F. P. and R. T. Barber (1987) An estimate of new production in the equatorial Pacific. *Deep-Sea Res.*, **34**, 1229-1243.

Cwienk, D. and M. Leinen (1985) Expression of global sediment component fluxes in surface sediment accumulation rates, *EOS, Transactions of the American Geophysical Union*, **66**, 930.

Emerson, S., and M. Bender (1981) Carbon fluxes at the sediment-water interface of the deep-sea: calcium carbonate preservation, *Journal of Marine Research*, **39**, 139-162.

Eppley, R. W. (1972) Temperature and phytoplankton growth in the sea. *Fisheries Bulletin*, **70**, 1063-1085.

Eppley, R. W. and B. Peterson (1979) Particulate organic matter flux and planktonic new production in the deep ocean. *Nature*, **282**,677-680.

Fernandez, E., P. Boyd, P. M. Holligan, and D. S. Harbour (1993) Production of organic and inorganic carbon within a large scale coccolithophore bloom in the North Atlantic ocean. Mar. Ecol. Prog. Ser., 97, 271-285.

Holligan, P. M. , M. Viollier, D. S. Harbour, P. Camus, and M. Champagne-Philippe (1983) Satellite and ship studies of coccolithophore production along a continental shelf edge, *Nature*, **304**, 339-342.

Holligan, P. M., E. Fernandez, J. Aiken, W. Balch, P. Boyd, P Burkill, M. Finch, S. Groom, G. Malin, K. Muller, D. Purdie, C. Robinson, C. Trees, S. Turner, and P. van der Wal (1993) A biogeochemical study of the coccolithophore, *Emiliania huxleyi*, in the north Atlantic, *Global Biogeochemical Cycles*, **7**, 879-900.

Holm-Hansen, O., C. J. Lorenzen, R. W. Holmes, and J. D. H. Strickland (1965) Fluorometric determination of chlorophyll. *J. Cons perm. int. Explor. Mer*, **30**, 3-15.

Honjo, S. (1976) Coccoliths: production, transportation and sedimentation. Mar. *Micropaleontology*, **1**, 65-79.

Honjo, S, J. Dymond, R. Collier, and S. J. Manganini (submitted) Export production of particles to the interior of the equatorial Pacific Ocean during the 1992 EqPac experiment, *Deep-Sea Research.*

Kawaguti, S. and D. Sakumoto (1948) The effect of light on the calcium deposition of corals. *Bulletin of the Oceanographic Institite of Taiwan*, **4**, 65-70.

Kilpatrick, K., W. M. Balch, Y. Ge, and K. J. Voss (1994) A photometer for the continuous measurement of calcite-dependent light scatter in seawater. *Proceedings of the Society of Photo-Optical Instrumentation Engineers*, in press.

Kramer, D. D. and J. H. Ryther (1960) The iron requirement of some marine plankton algae. *Biological Bulletin*, **119**, 324.

Lohmann, H. (1908) On the relationship between pelagic deposits and marine plankton (in German), *Int. Rev. Ges. Hydrobiol. Hydrogr.*, **1**, 309-323.

Margalef, Ramon (1978) Life-forms of phytoplankton as survival alternatives in an unstable environment, *Oceanologica Acta*, **1**, 493-509.

McIntyre, A. and A.W.H. Be (1967) Modern coccolithophoridae of the Atlantic Ocean-I. Placoliths and cyrtoliths. *Deep Sea Research*, **14**, 561-597.

Millero, F. J. and A. Poisson (1981) International one-atmosphere equation of state of sea-water, *Deep-Sea Research*, **28A**, 625-629.

Milliman, J. D. (1993) Production and accumulation of calcium carbonate in the ocean: budget of a nonsteady state. Global Biogeochemical Cycles, **7**, 927-957.

Morel, A. and Y. Ahn (1991) Optics of heterotrophic nanoflagellates and ciliates: A tentative assessment of their scattering role in oceanic waters compared to those of bacterial and algal cells. *Journal of Marine Research*, **49**, 177-202.

Okada, H. and S. Honjo (1973) The distribution of oceanic coccolithophorids in the Pacific. Deep-Sea Research, **20**, 355-374.

Okada, H. and A. McIntyre (1977) Modern coccolithophores of the Pacific and North Atlantic Oceans. Micropaleontology, **23**, 1-55.

Paasche, E. (1962) Coccolith formation. *Nature*, **193**, 1094-1095.

Paasche, E. (1963) The adaptation of the Carbon-14 method for the measurement of coccolith production in *Coccolithus huxleyi*, *Physiologia Plantarum*, **16**, 186-200.

Parsons, T. R., Y. Maita and C. M. Lalli (1984) *A manual of chemical and biological methods for seawater analysis*. Pergamon Press Inc., New York, 173 pp.

Pena, M. A., M. R. Lewis, and J. J. Cullen (1994) New production in the warm waters of the tropical Pacific Ocean. *Journal of Geophysical Research*, **99**, 14255-14268.

Reid, F (1980) Coccolithophorids of the North Pacific Central Gyre with notes on their vertical and seasonal distribution. *Micropaleontology*, **26**, 151-176.

Sarnthein, M., K. Winn, J.-C. Duplessy and M.R. Fontugne (1988) Global carbon variations of surface ocean productivity in low and mid-latitudes: influence on CO2 reservoirs of the deep ocean and atmosphere during the last 21,000 years. *Paleo-oceanography*, **3**, 361-399.

Seibold, E. and W. H. Berger (1982) *The sea floor- An introduction to marine geology*. Springer-Verlag, New York, 288pp.

ter Kuile, B. and J. Erez. (1987) Uptake of inorganic carbon and internal carbon cycling in symbiont-bearing benthonic foraminifera, *Marine Biology*, **94**, 499-509.

Van Andel, T. H. (1975) Cenozoic history and paleoceanography of the central equatorial Pacific Ocean, *Geological Society of America Memoirs*, **143**, 1-134.

Wefer, G. (1980) Carbonate production by algae *Halimeda*, *Penicillus* and *Padina*. *Nature*, **285**, 323-324.

Westbroek, P, C. W. Brown, J. van Bleijswijk, C. Brownlee, G. Jan Brummer, M. Conte, J. Egge, E. Fernandez, R. Jordan, M. Knappertsbusch, J. Stefels, M. Veldhuis, P. van der Wal and J. Young (1993) A model system approach to biological climate forcing. The example of *Emiliania huxley*i, *Global and Planetary Change*, **8**, 27-46.

Wyrtki, K. (1981) An estimate of equatorial upwelling in the Pacific. *Journal of Physical Oceanography*, **11**, 1205-1214.

Yentsch, C. S. and D. Menzel (1963) Method for the determination of phytoplankton chlorophyll and phaeophytin by fluorescence. *Deep-Sea Research*, **10**, 221-231.

Yoder, J. A., S. G. Ackleson, R. T. Barber, P. Flament and W. M. Balch (1994) A line in the sea. Nature, **371**, 689-692.

Figure Legend

Fig. 1. (a) Vertical section of detached coccolith concentration from 12°N to 12°S, from the surface to 120m depth, along $140^0$ W. Contour levels are 50, 100, 200, 400, and 600 $ml^{-1}$. Counts are made as described in text. (b) Vertical section of total plated coccolithophores, showing contours of 5,10, 20, 40, and 60 $ml^{-1}$. Sample locations and depths are shown with an asterisk in both panels.

Fig. 2. Plot of detached coccoliths versus total plated coccolithophores (log axes). Formula for the least-squares fit line is given in the text.

Fig. 3. Vertical section along $140^0$ W for unidentified, 0.5μM diameter, birefringent particles (possibly holococcoliths). Other details of the section are described in Fig. 1. Contour interval is $0.4 \times 10^4$, $2.0 \times 10^4$, $3.6 \times 10^4$, $5.2 \times 10^4$, $6.8 \times 10^4$ particles per mL.

Fig. 4. (a) Vertical section of photosynthesis along $140^0$ W. Other details of section are described in Fig. 1. Contour intervals are: 0.15, 0.40, 0.65, 0.90, 1.15, 1.40, 1.65, 1.90, 2.15 mmol C $m^{-3}$ $d^{-1}$. (b) Vertical section of calcification from same samples as in panel a above. Contour intervals are: $8.3 \times 10^{-3}$, $16.7 \times 10^{-3}$, $33.3 \times 10^{-3}$, $66.7 \times 10^{-3}$ mmol C $m^{-3}$ $d^{-1}$. Peak calcification values (above $66.7 \times 10^{-3}$ mmol C $m^{-3}$ $d^{-1}$) are designated. (c) Vertical section of suspended calcite carbon showing contours of 0.17, 0.25, 0.33, 0.67, 1.33 mmol calcite C $m^{-3}$.

Fig. 5. Calcification rate (mmol C $m^{-3}$ $d^{-1}$) versus photosynthesis (mmol C $m^{-3}$ $d^{-1}$) for all data from TT011. The 1:1 line is shown for reference. It can be seen that in some cases, calcification rates were equal to photosynthesis rates but generally, they were about 10% of the photosynthesis rates and this fraction varied considerably. Symbols on the figure are: + and * = in situ replicates, Δ and o = simulated in situ replicates.

Fig. 6. (a) Integrated photosynthesis and calcification versus latitude along 140°W. (Symbols are: + = in situ photosynthesis, * = simulated in situ photosynthesis, o = in situ calcification and Δ= simulated in situ calcification; units are mmol C $m^{-2}$ $d^{-1}$). (b) Integrated suspended calcite (molC $m^{-2}$). Results were integrated to 120m depth for both plots. Samples from 7° N-12° N were lost. (c) Turnover time of euphotic zone calcite carbon (days) versus latitude. Values calculated by dividing the standing stock of calcite by

the calcification rate. Symbols are: + = simulated in situ incubations and o= in situ incubations.

Fig. 7. Integral calcification as a percent of the total carbon fixed, based on integrals of the simulated in situ incubation data.

Fig. 8. Plot of the concentration of detached coccoliths versus the estimated surface area of plated coccolithophores. The coccolith concentration does not include those attached to cells or in loose clumps. The cell surface area was calculated by binning the counts of plated cells into nominal size categories, then calculating surface area assuming spherical cells. See text for details. The expected relationship for 1 μm, 2μm, 4μm, and 8μm radius coccoliths is shown, which assumes that the coccoliths were shed as a single layer, that they were round discs, and that the detached plates originally completely covered the cells. These data suggest calcite particles of 1-8μm in radius. It was not possible to accurately include "clumped" coccoliths into this calculation which would have shifted the data to the right on the plot.

Fig. 9. Vertical section along 140° W of the extracellular calcite flux, as determined from the $^{14}C$ incorporation data and binned cell counts (units are mol C ( $m^{-2}$ cell surface area) $d^{-1}$ ).

Fig. 10. Surface transect data along 140° W for (a) salinity and chlorophyll, (b) temperature and total $\beta_{90}$ volume scatter and (c) calcite-dependent $\beta_{90}$ (acid labile). Each plot contains 2726 measurements between 12° N and 12° S (no data were collected between 5° N and 3° N due to instrument problems). The average data collection rate was 1.1 points per kilometer.

Fig. 11. Surface transect data plotted on 2 dimensional temperature-salinity diagrams to allow better water mass discrimination. (a) Temperature-salinity data showing isopleths of density calculated from equations of Millero and Poisson (1981). (b) Same data as in panel a showing contours of latitude. (c) Distribution of chlorophyll within the various water masses surveyed, also showing isopleths of latitude as in panel b. (d) Distribution of calcite-dependent $\beta_{90}$ within the various water masses surveyed, also showing isopleths of latitude as in panel b. (e)Distribution of total $\beta_{90}$ within the various water masses surveyed, also showing isopleths of latitude as in panel b.

Fig. 12. Surface transect data for total $\beta_{90}$ versus temperature. Upper and lower dashed lines were drawn by eye to illustrate curvilinear data envelope.

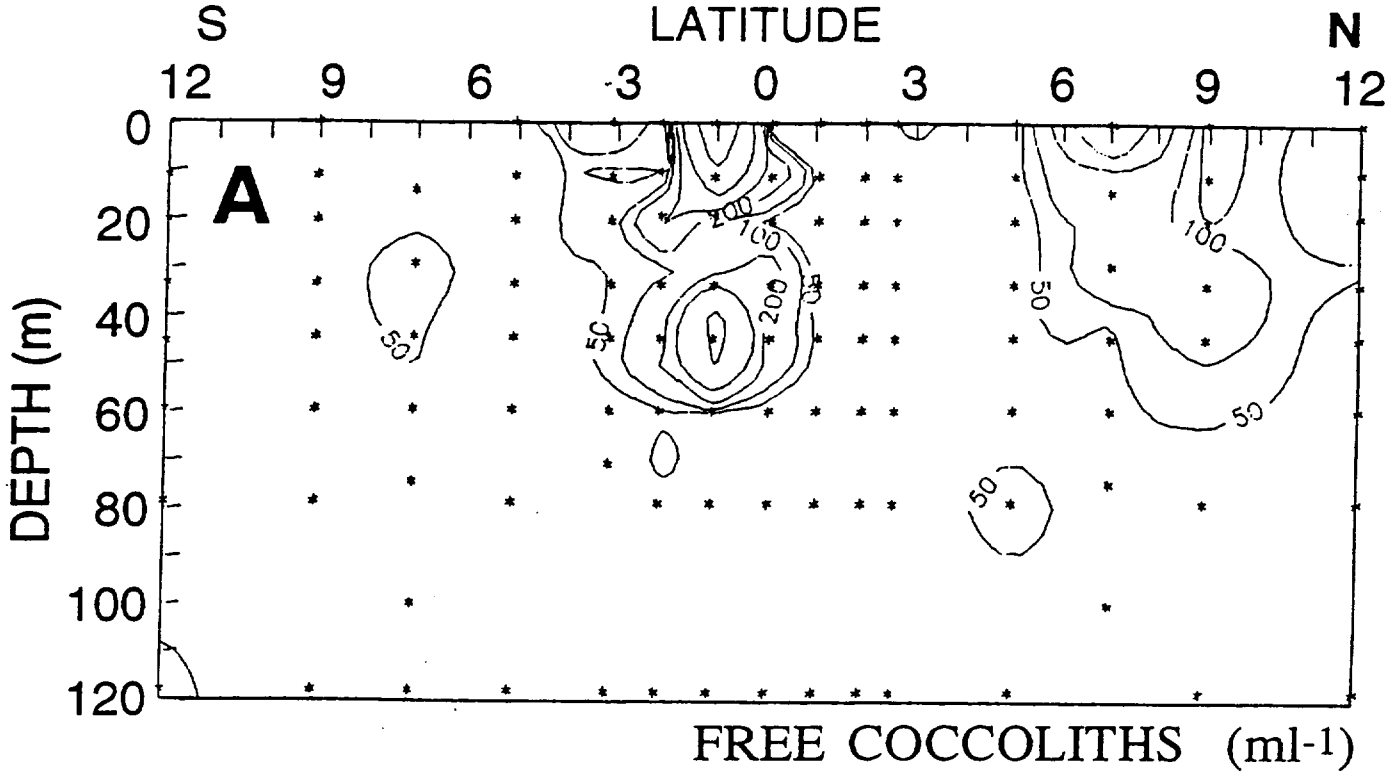
S
LATITUDE
N
12 9 6 3 0 3 6 9 12
A
DEPTH (m)
0 20 40 60 80 100 120
FREE COCCOLITHS (ml-1)

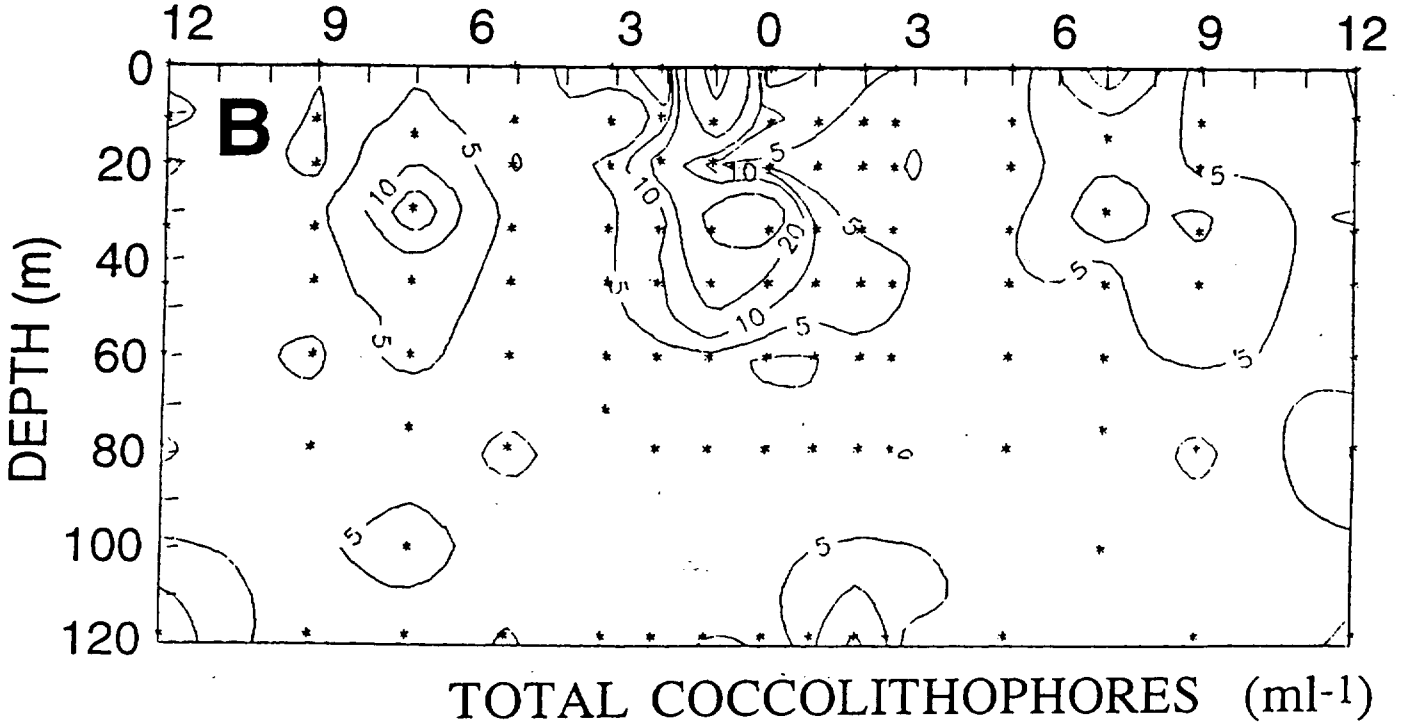
12 9 6 3 0 3 6 9 12
B
DEPTH (m)
0 20 40 60 80 100 120
TOTAL COCCOLITHOPHORES (ml-1)

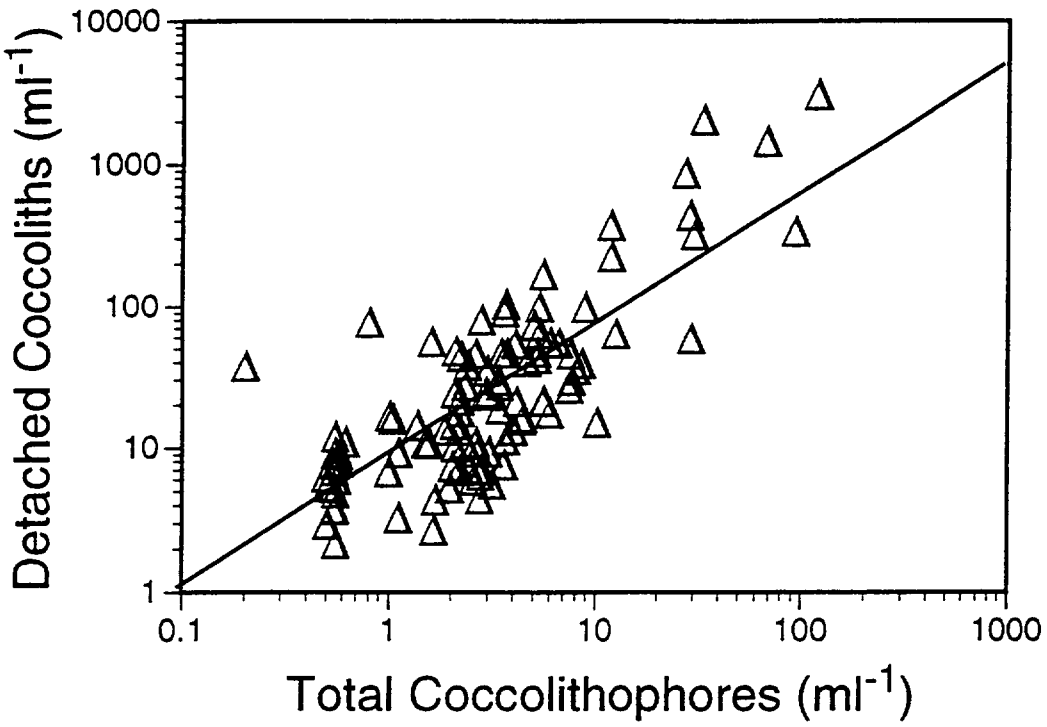
Detached Coccoliths (ml-1)
10000
1000
100
10
1
0.1
1
10
100
1000
Total Coccolithophores (ml-1)

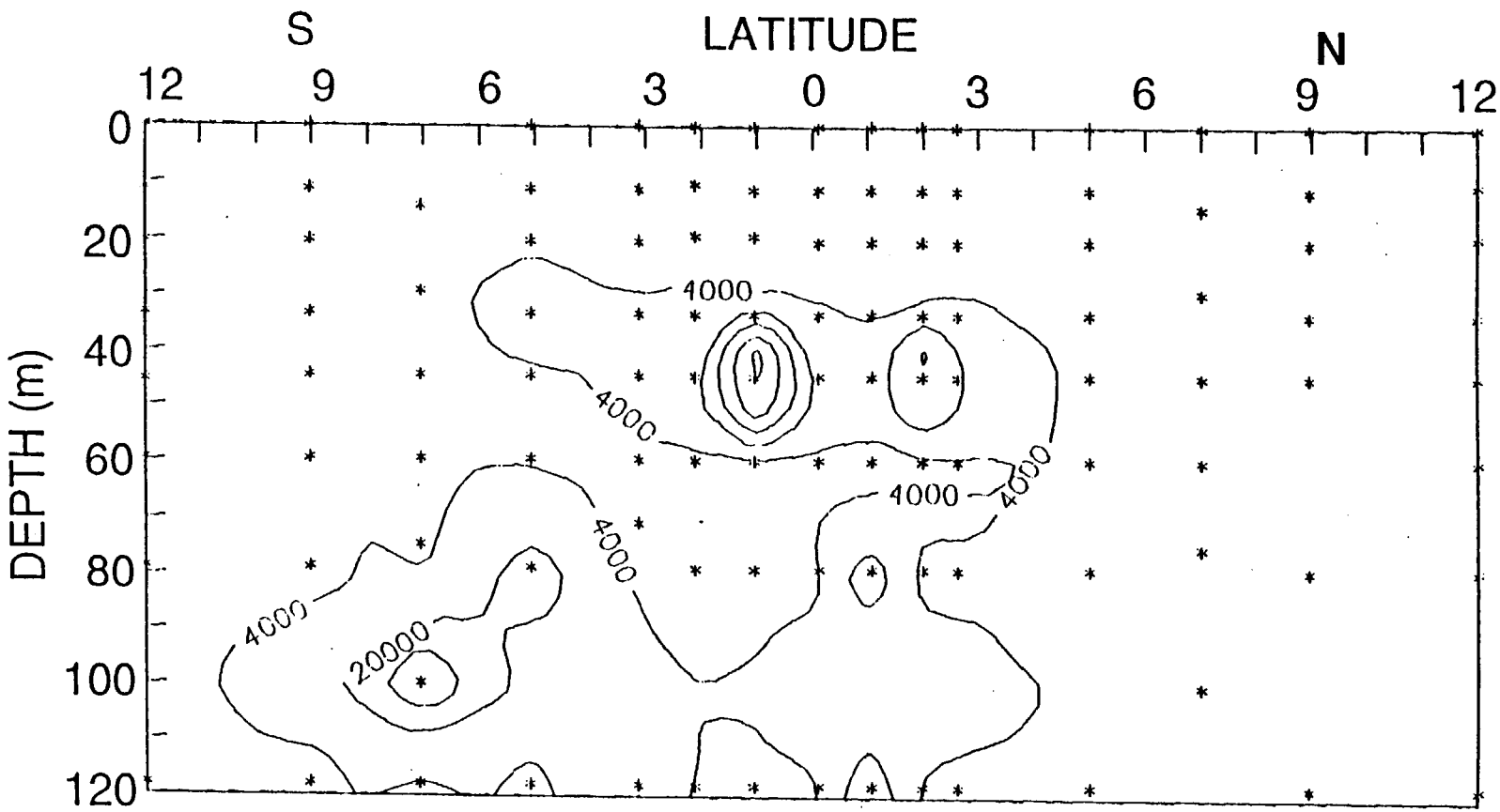
S
LATITUDE
N
12
9
6
3
0
3
6
9
12
0
20
40
60
80
100
120
DEPTH (m)
4000
4000
4000
4000
4000
20000

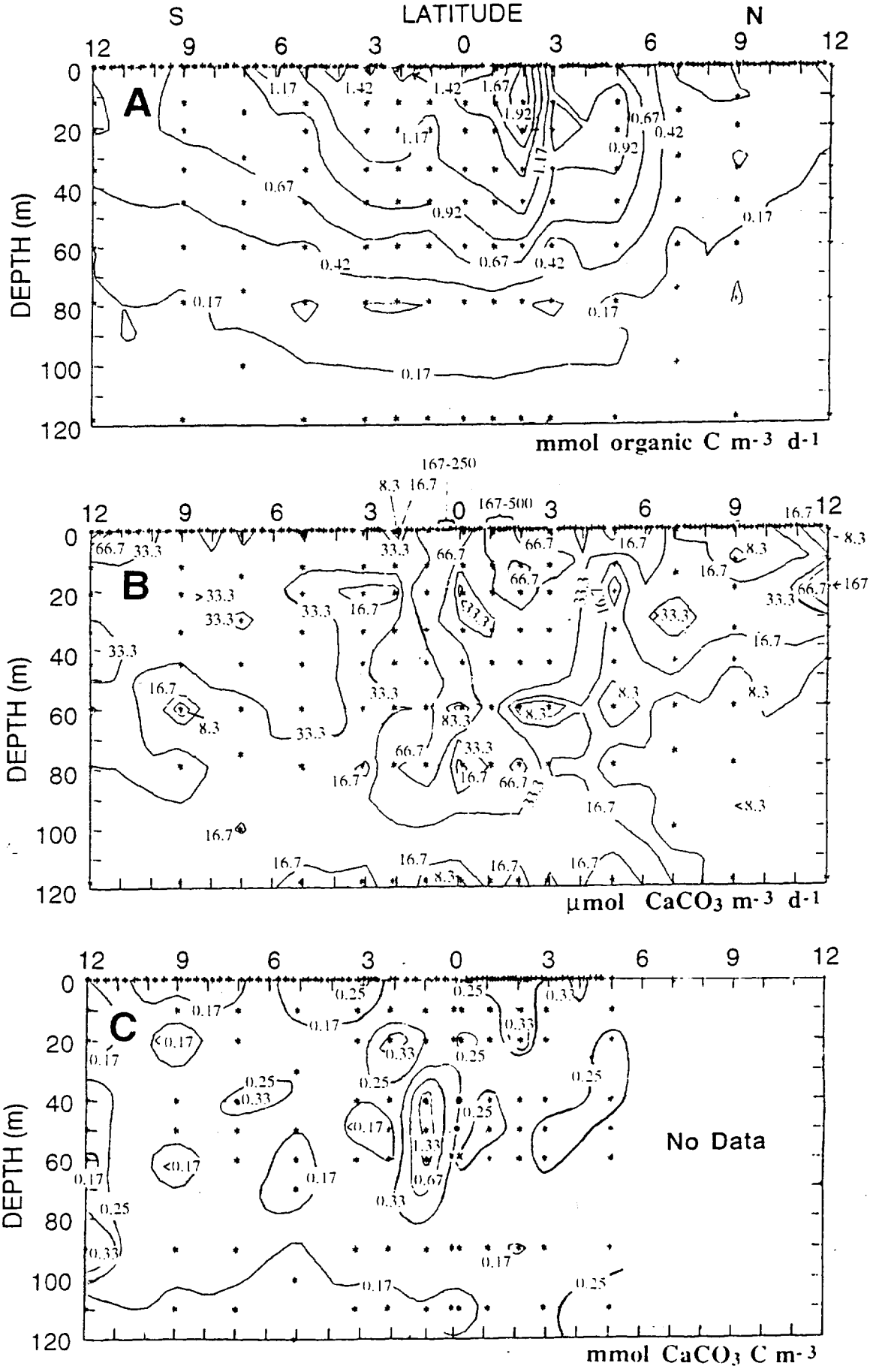
S
LATITUDE
N
12 9 6 3 0 3 6 9 12
0 20 40 60 80 100 120
DEPTH (m)
A
mmol organic C m-3 d-1
B
167-250
167-500
µmol CaCO3 m-3 d-1
C
No Data
mmol CaCO3 C m-3

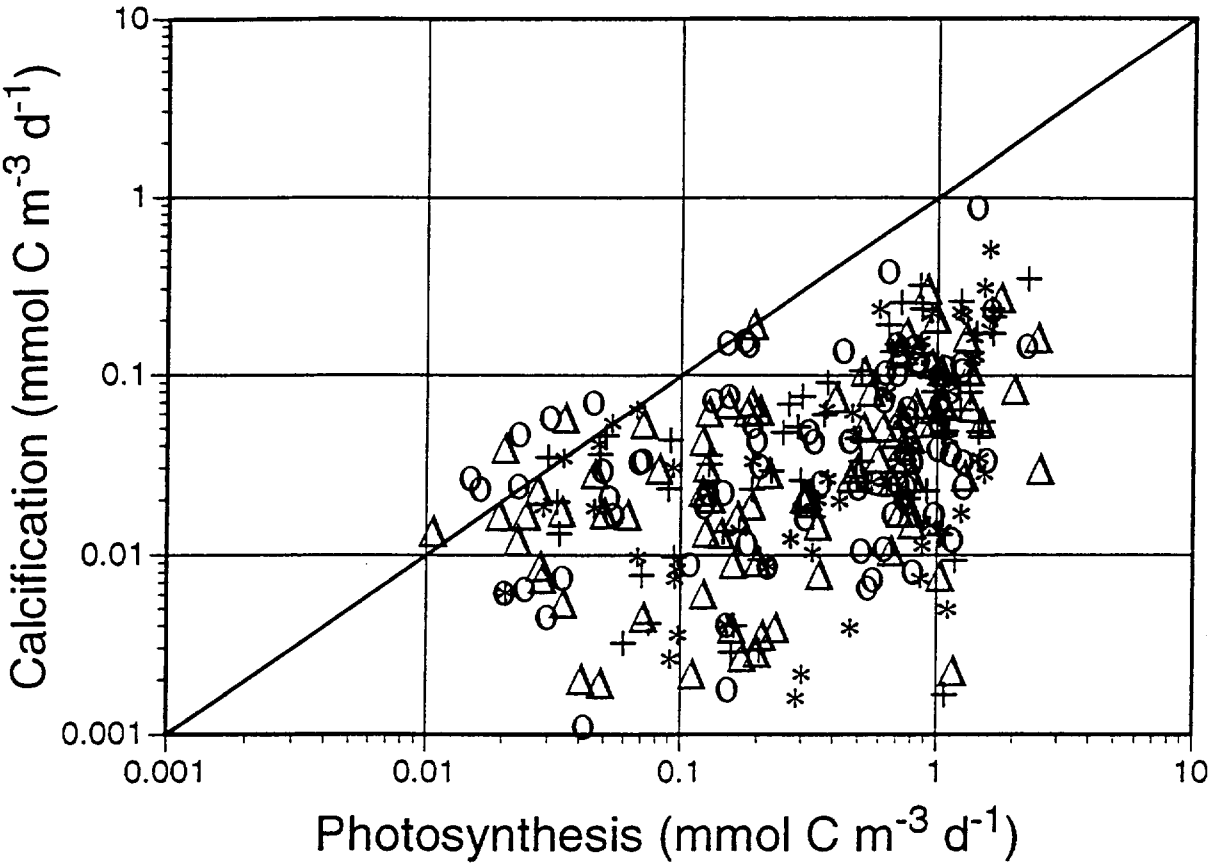
Calcification (mmol C m-3 d-1)
Photosynthesis (mmol C m-3 d-1)
10
1
0.1
0.01
0.001
0.001
0.01
0.1
1
10

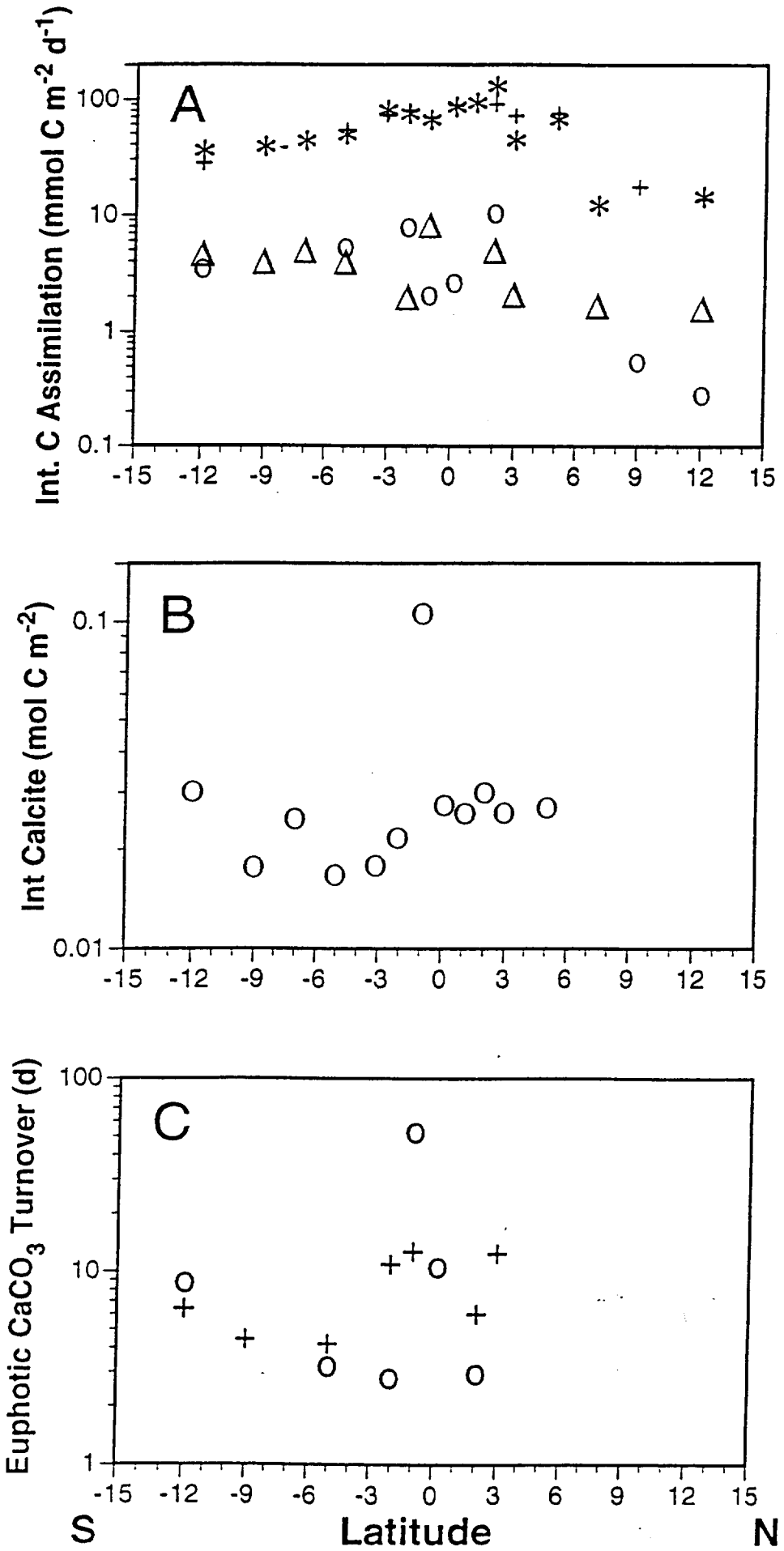
A
Int. C Assimilation (mmol C m-2 d-1)
100
10
1
0.1
-15 -12 -9 -6 -3 0 3 6 9 12 15
B
Int Calcite (mol C m-2)
0.1
0.01
-15 -12 -9 -6 -3 0 3 6 9 12 15
C
Euphotic CaCO3 Turnover (d)
100
10
1
-15 -12 -9 -6 -3 0 3 6 9 12 15
S
Latitude
N

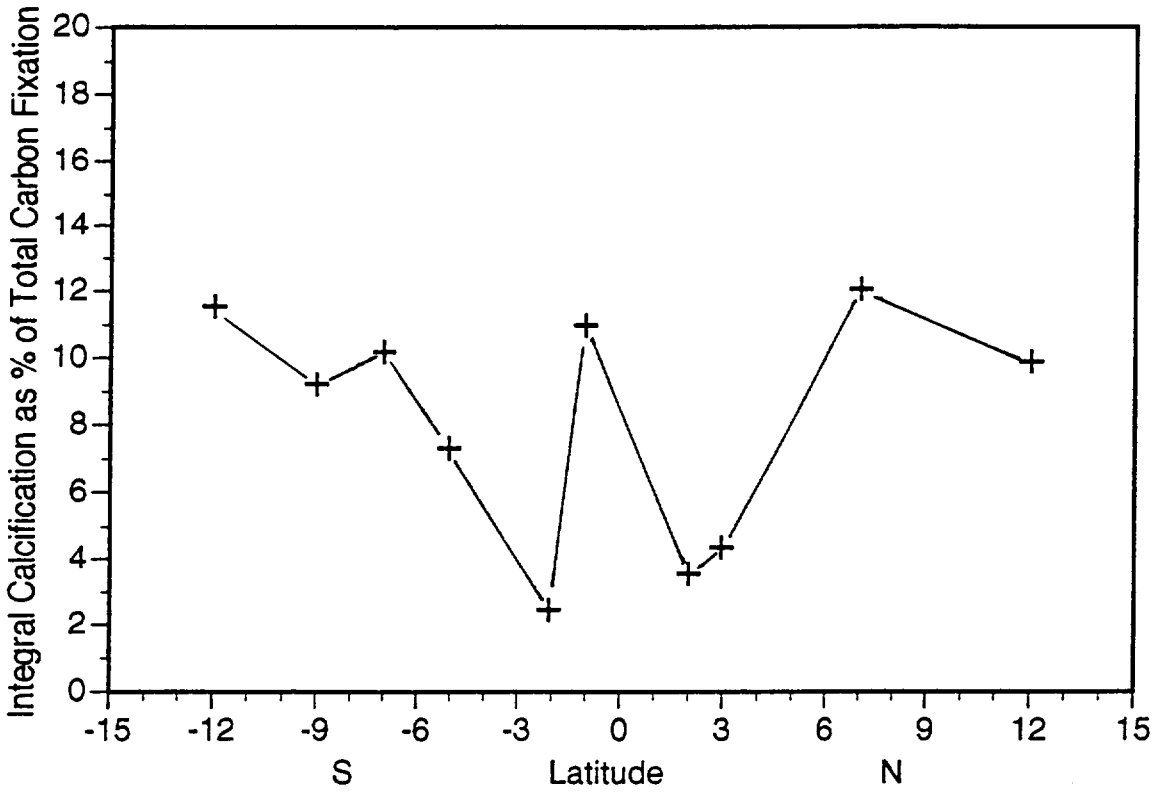


Simulated In Situ Data

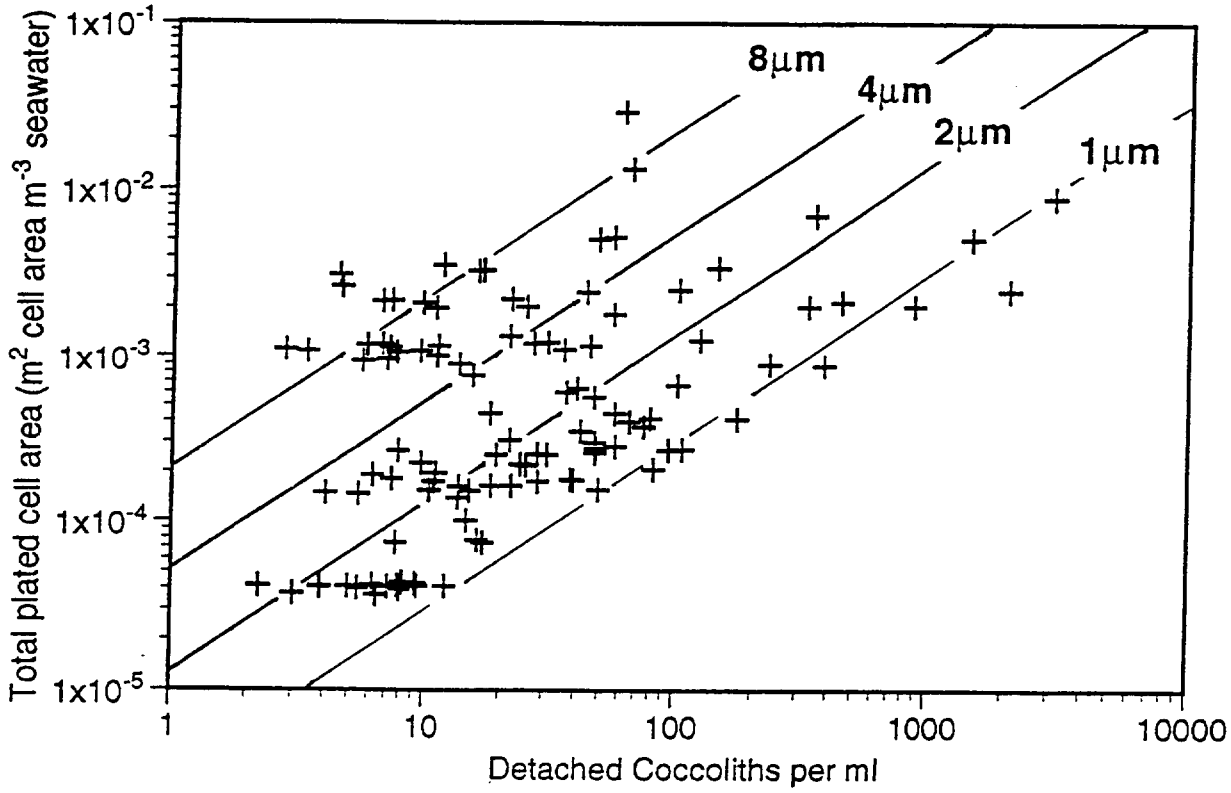
8μm
4μm
2μm
1μm
Total plated cell area (m² cell area m⁻³ seawater)
1x10⁻¹
1x10⁻²
1x10⁻³
1x10⁻⁴
1x10⁻⁵
1
10
100
1000
10000
Detached Coccoliths per ml

# Extracellular Calcite Flux

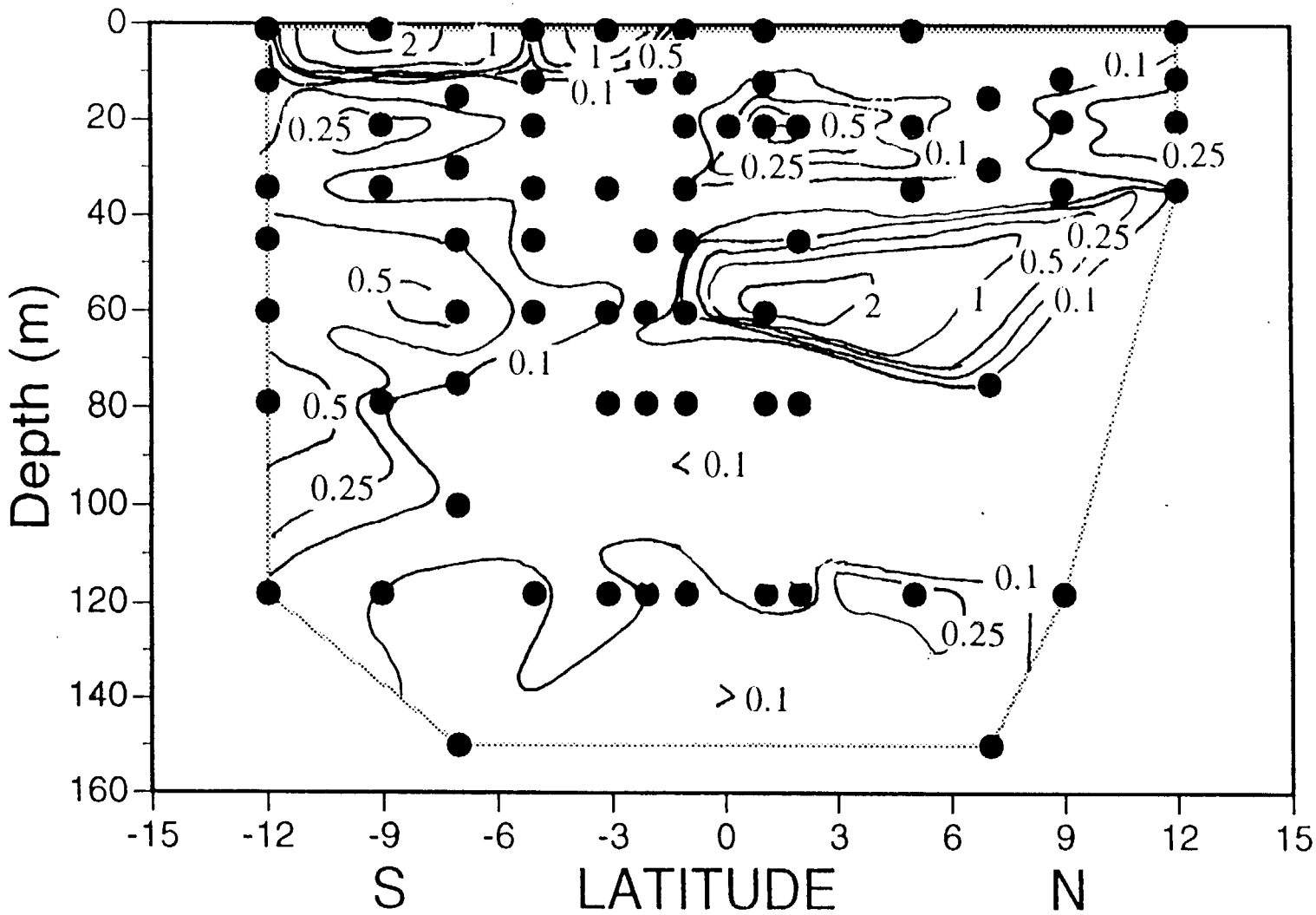


Fig 9

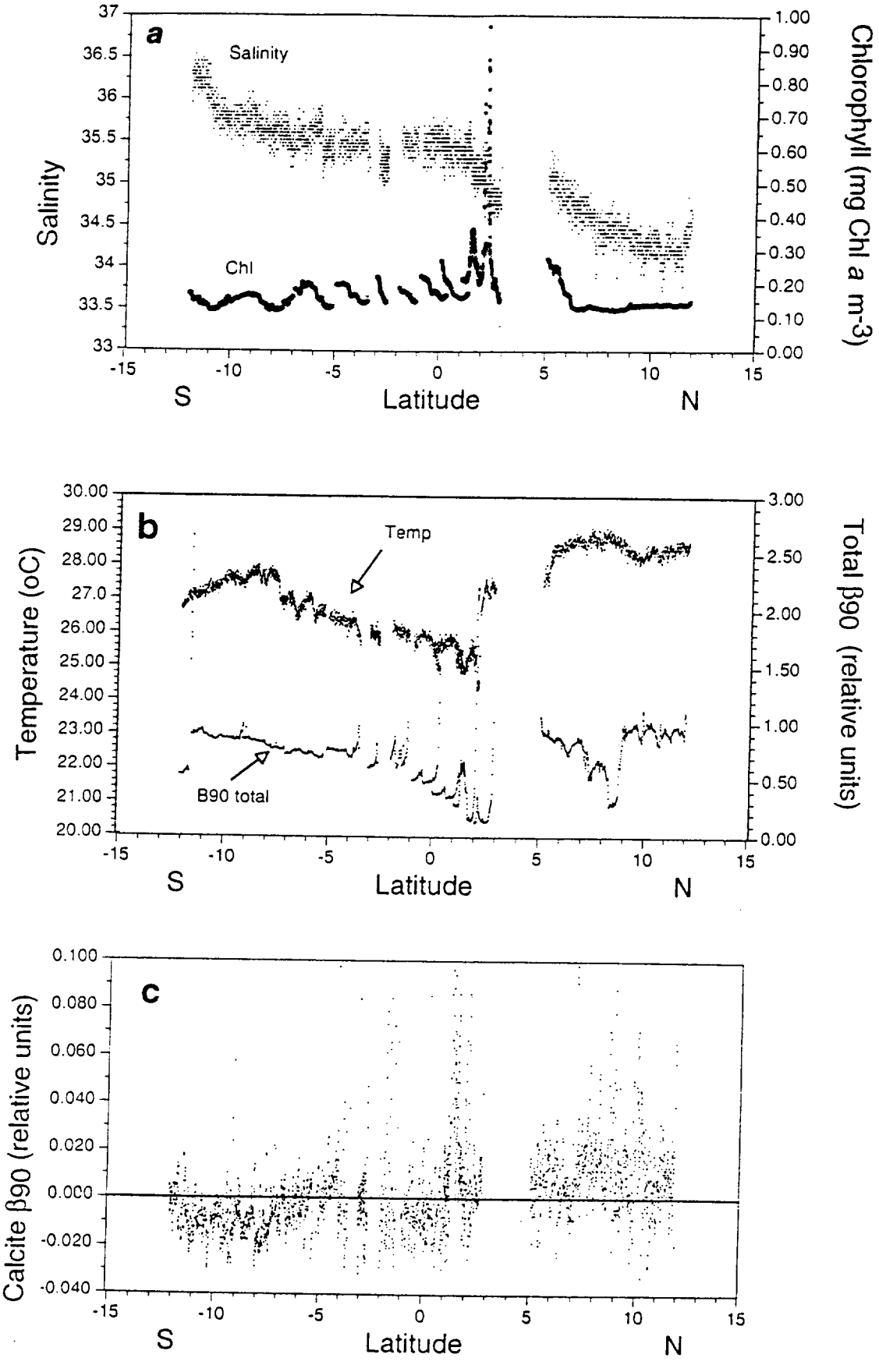
a
Salinity
Chl
Salinity
Chlorophyll (mg Chl a m-3)
37
36.5
36
35.5
35
34.5
34
33.5
33
1.00
0.90
0.80
0.70
0.60
0.50
0.40
0.30
0.20
0.10
0.00
-15
-10
-5
0
5
10
15
S
Latitude
N
b
Temp
B90 total
Temperature (oC)
Total β90 (relative units)
30.00
29.00
28.00
27.0
26.00
25.00
24.00
23.00
22.00
21.00
20.00
3.00
2.50
2.00
1.50
1.00
0.50
0.00
S
Latitude
N
c
Calcite β90 (relative units)
0.100
0.080
0.060
0.040
0.020
0.000
-0.020
-0.040
S
Latitude
N

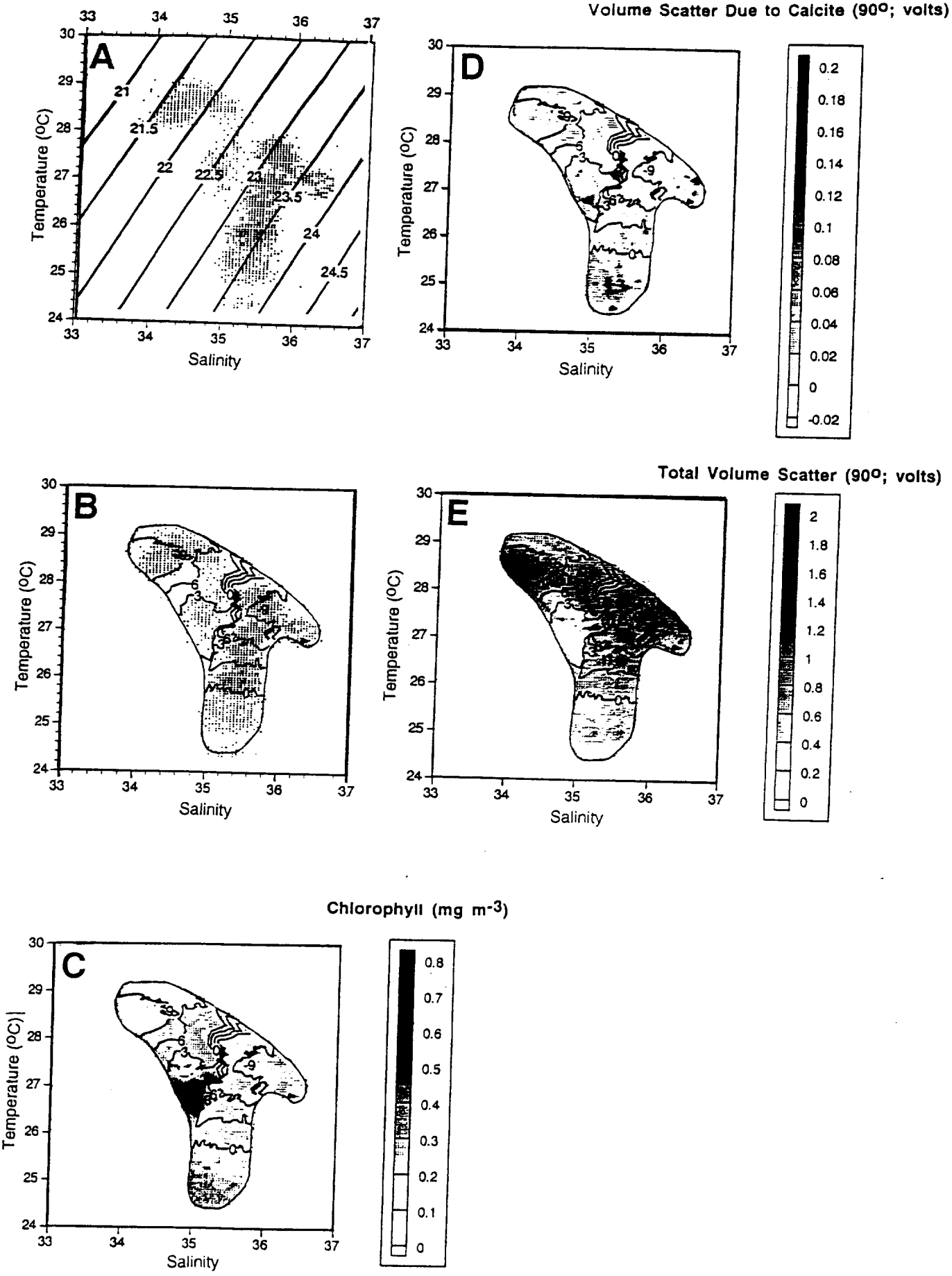
A
B
C
D
E
Temperature (°C)
Salinity
21
21.5
22
22.5
23
23.5
24
24.5
Volume Scatter Due to Calcite (90°; volts)
0.2
0.18
0.16
0.14
0.12
0.1
0.08
0.06
0.04
0.02
0
-0.02
Total Volume Scatter (90°; volts)
2
1.8
1.6
1.4
1.2
1
0.8
0.6
0.4
0.2
0
Chlorophyll (mg m-3)
0.8
0.7
0.6
0.5
0.4
0.3
0.2
0.1
0

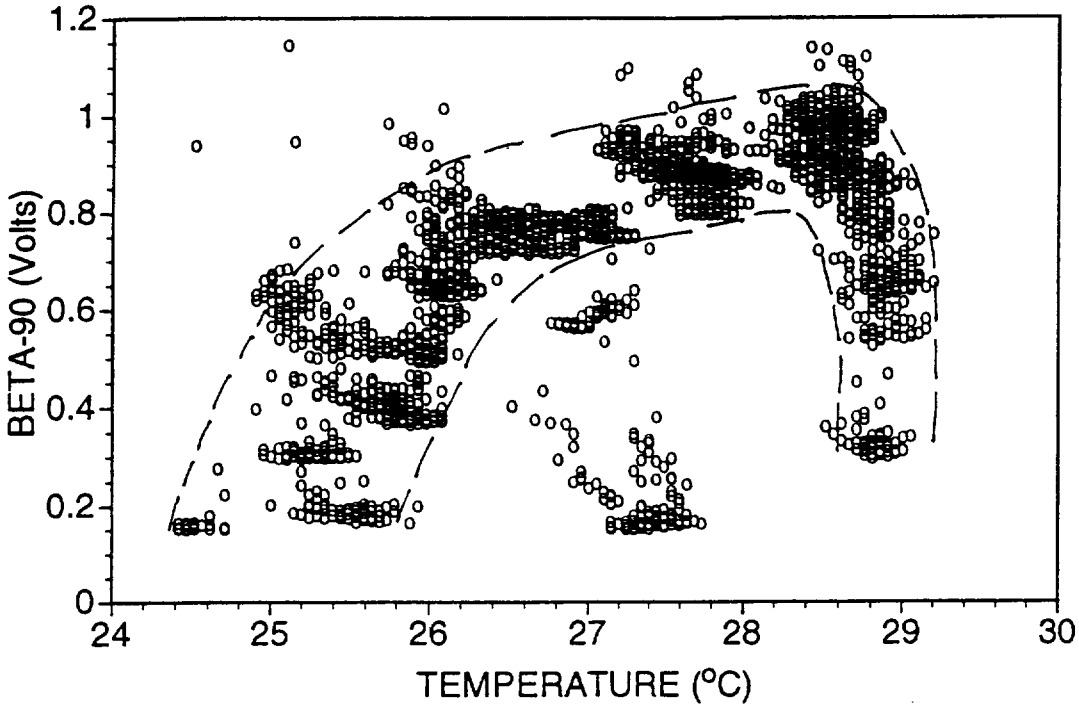
1.2
1
0.8
0.6
0.4
0.2
0
BETA-90 (Volts)
24
25
26
27
28
29
30
TEMPERATURE (°C)